SUPPORTING INFORMATION

Synergism among Polydispersed Amphiphilic Block Copolymers Leading to Spontaneous Physical Hydrogelation upon Heating

Shuquan Cui[1)], Liang Chen[1)], Lin Yu[1,2)], Jiandong Ding[1,2)] *

[1)] State Key Laboratory of Molecular Engineering of Polymers, Department of Macromolecular Science, Fudan University, Shanghai 200438, China

[2)] Zhuhai Fudan Innovation Institute, Zhuhai, Guangdong 519000, China

* Corresponding author. E-mail address: jdding1@fudan.edu.cn (J.D. Ding)

S1. SUPPLEMENTARY METHODS

S1.1 Relaxation process in simulations of lattice chains

As schematically shown in Figure S1, Larson model with a permitted bond length of 1 or $\sqrt{2}$ (in unit of lattice size) was employed as the micro-relaxation mode in our dynamic Monte Carlo simulations, and a partial reptation model was also used to promote the simulation efficiency. Metropolis sampling was chosen as the sampling method.

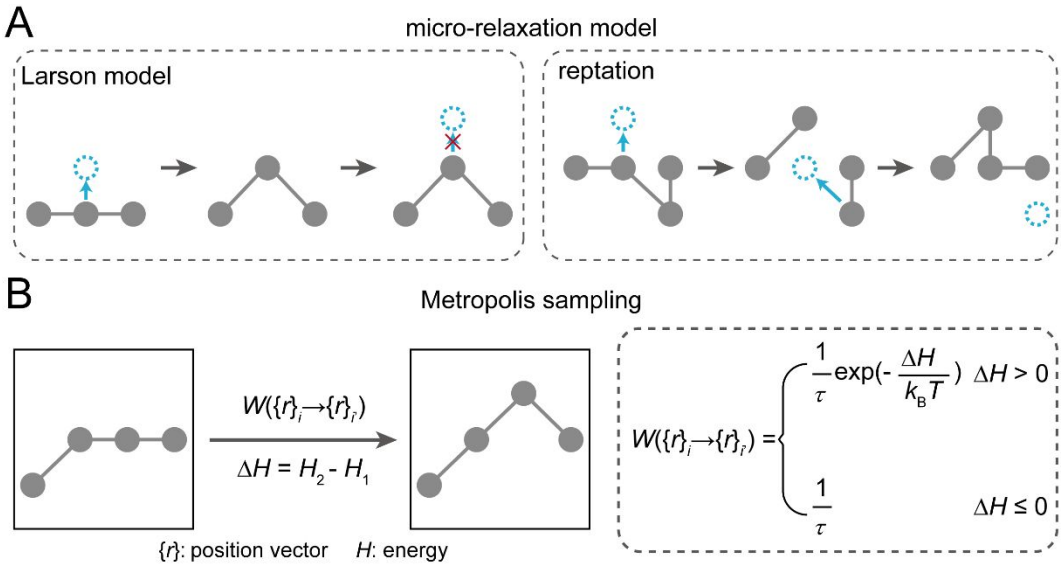

Figure S1. Micro-relaxation model and sampling method in simulations. (A) Larson model and partial reptation model; (B) Metropolis sampling method.

The general relaxation process in simulations can be described as follows:

(1) By a random number produced on a computer for a simulation on two-dimensional lattices, a bead in the system was selected. One of the eight nearest neighbor and next-nearest neighbor sites relative to the selected bead was also randomly selected. The exchange was attempted if the selected site was a vacancy.

(2) Three types of exchanges might happen. If an exchange did not break the chain (lengths of both new-formed bonds $\leq \sqrt{2}$), the attempt was permitted (a single movement, Larson model). If an exchange created a single break (one new-formed bond length $\leq \sqrt{2}$, and the other bond length $> \sqrt{2}$), the vacancy would continue to exchange with the subsequent beads along the chain until the chain reconnection (a cooperative movement, reptation). In the cases of both new-formed bonds lengths $> \sqrt{2}$, the exchange broke two connections and must be forbidden. Besides, the bond crossing was not allowed in any micro-relaxation of self-avoiding chains.

(3) The attempted micro-relaxation led to two states, an old state before exchanging (state 1, with energy H_1) and a new one after exchanging (state 2, with energy H_2). The energy change (ΔH) between the two states reads $\Delta H = H_2 - H_1$. If $\Delta H \leq 0$, the new state was accepted. Otherwise, the new state was accepted only with a probability $\exp(-\Delta H/k_B T)$, where k_B is the Boltzmann constant, and T is the Kelvin temperature.

S1.2 Chain parameters in simulations

The default chain parameters of systems with $Đ_M$ from hydrophobic blocks are presented in Figure S2. For convenience, P1, P2, and P3 represent the short (low MW) chain ($A_2B_8A_2$), the medium (medium MW) chain ($A_{28}B_8A_{28}$), and the long (high MW) chain ($A_{54}B_8A_{54}$).

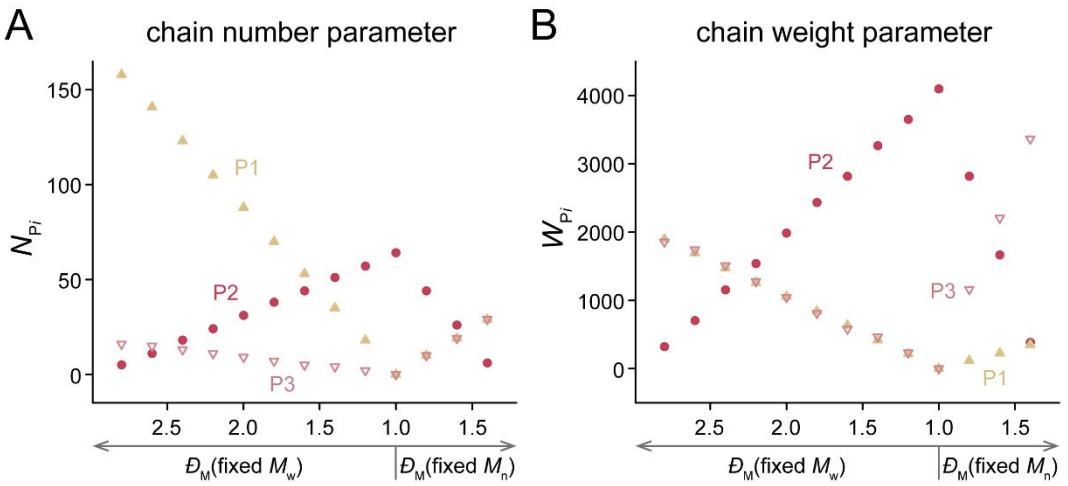

Figure S2. Default chain parameters utilized in simulated systems with $Đ_M$ from hydrophobic blocks. (A) Chain number parameters; (B) Chain weight parameters. In these systems, $\varphi = 0.25$.

S2. SUPPLEMENTARY RESULTS

S2.1 Evolution of multiple chains with simulation time

The convincing thermodynamic parameters should be counted after the system reaches equilibrium. In a dynamic Monte Carlo simulation, the system tends to equilibrate over time. We employed some typical parameters to characterize the system evolution. The results of representative systems are shown in Figure S3. Both at the athermal state and at the predetermined temperatures, the typical parameters became stable in a relatively short time in our simulations, indicating the achievement of the equilibrium efficiently.

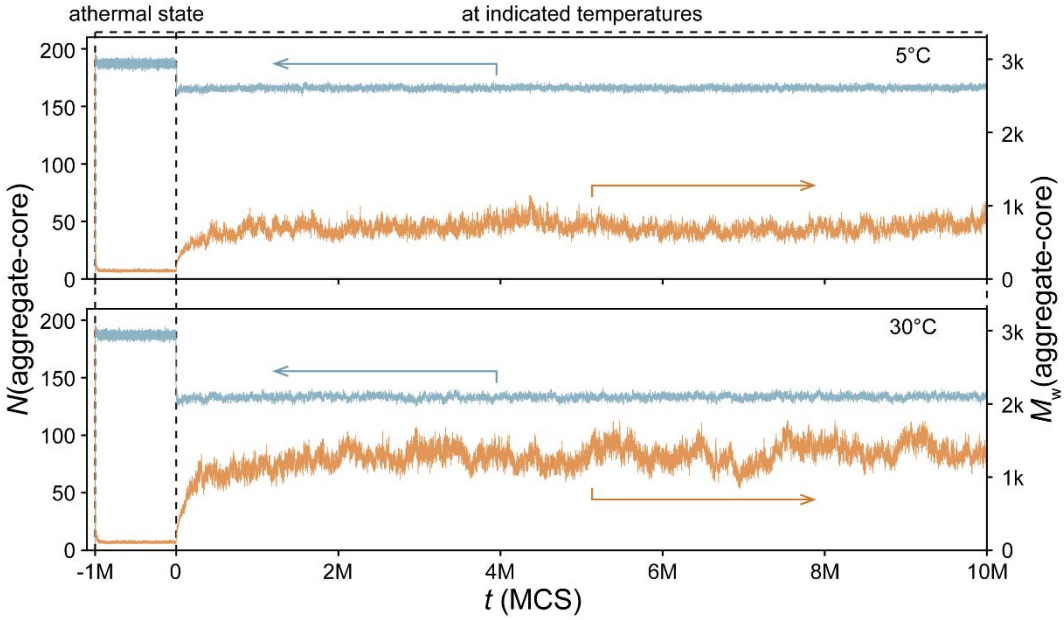

Figure S3. Evolutions of the number of aggregate-core N(aggregate-core) and weight average molecular weight of aggregate-core M_w(aggregate-core) with time in Monte Carlo simulations. The unit of time in simulations was Monte Carlo step (MCS). The data was collected from a system ($Đ_M$(fixed M_w) = 2.2 and φ = 0.25) with the default chain models.

For a visual understanding, the evolutions of systems are exhibited by the corresponding snapshots, as presented in Figure S4.

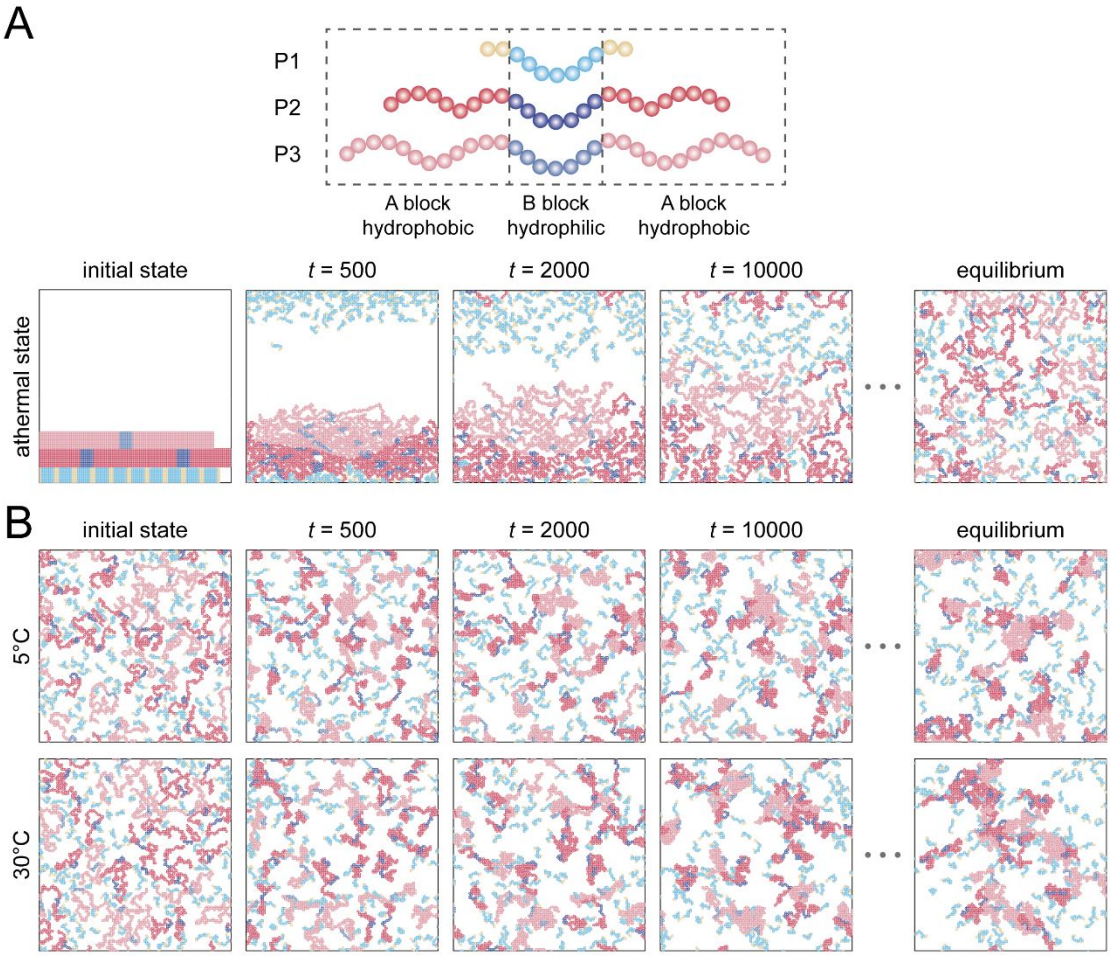

Figure S4. The evolution process of typical simulated systems. The unit of time was MCS. (A) Schematic of the model copolymers and the snapshots at indicated times at the athermal state. Here for clarity, the bead number of the schematic chain model is shown less than that of the simulated model; (B) Snapshots at different times at 5°C and 30°C. The equilibrium states for the athermal state and systems with the indicated temperatures were obtained after t = 500000 MCS and t = 5000000 MCS, respectively. The system here was the same as in Figure S3.

S2.2 Snapshot of the gel network

For observing the gel network intuitively, a typical snapshot of the thermogel as well as the snapshot only showing the hydrophobic beads is presented in Figure S5. Obviously, the aggregation of the hydrophobic beads promoted the formation of the

gel network.

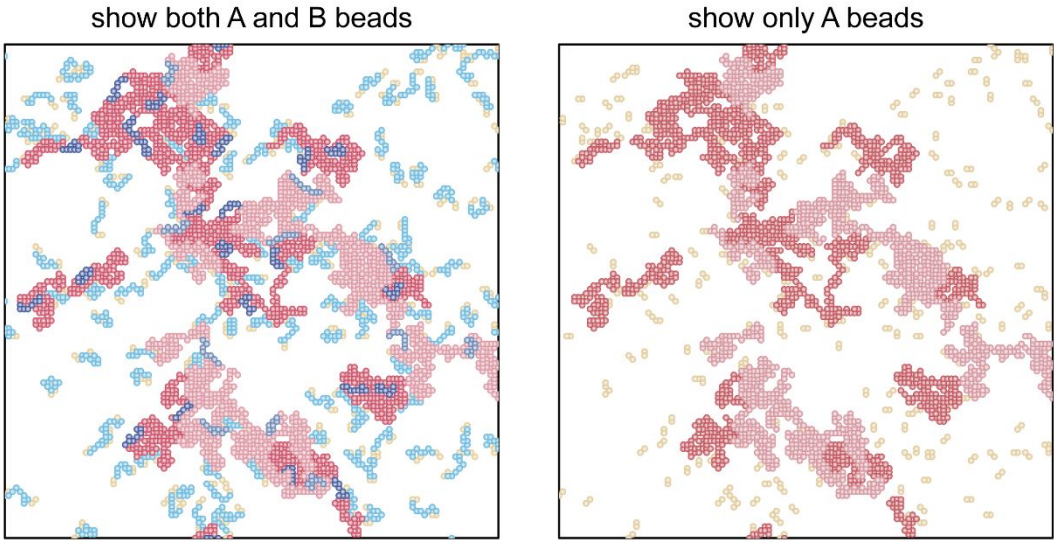

Figure S5. Network structure of the thermogel in a polydispersed system. (Left) Typical snapshot of the thermogel; (Right) Typical snapshot of the thermogel only showing the hydrophobic beads. In this system, $Đ_M$(fixed M_w) = 2.2 and φ = 0.25. The temperature was 30°C (higher than the T_{gel} in this system). Chain models here were the default model chains.

S2.3 Aggregate size distribution at different temperatures

The terms of aggregate-total and aggregate-core were described in the main manuscript. The size of an aggregate-core was defined as the total beads of the AB semi-chains belonging to it (e.g., an $A_{28}B_8A_{28}$ chain corresponded to two $A_{28}B_4$ semi-chains). For aggregate-total, its size corresponded to the total beads of ABA model chains it contained. The distribution of aggregate size in simulated systems could be quantitatively analyzed, and the results are presented in Figure S6.

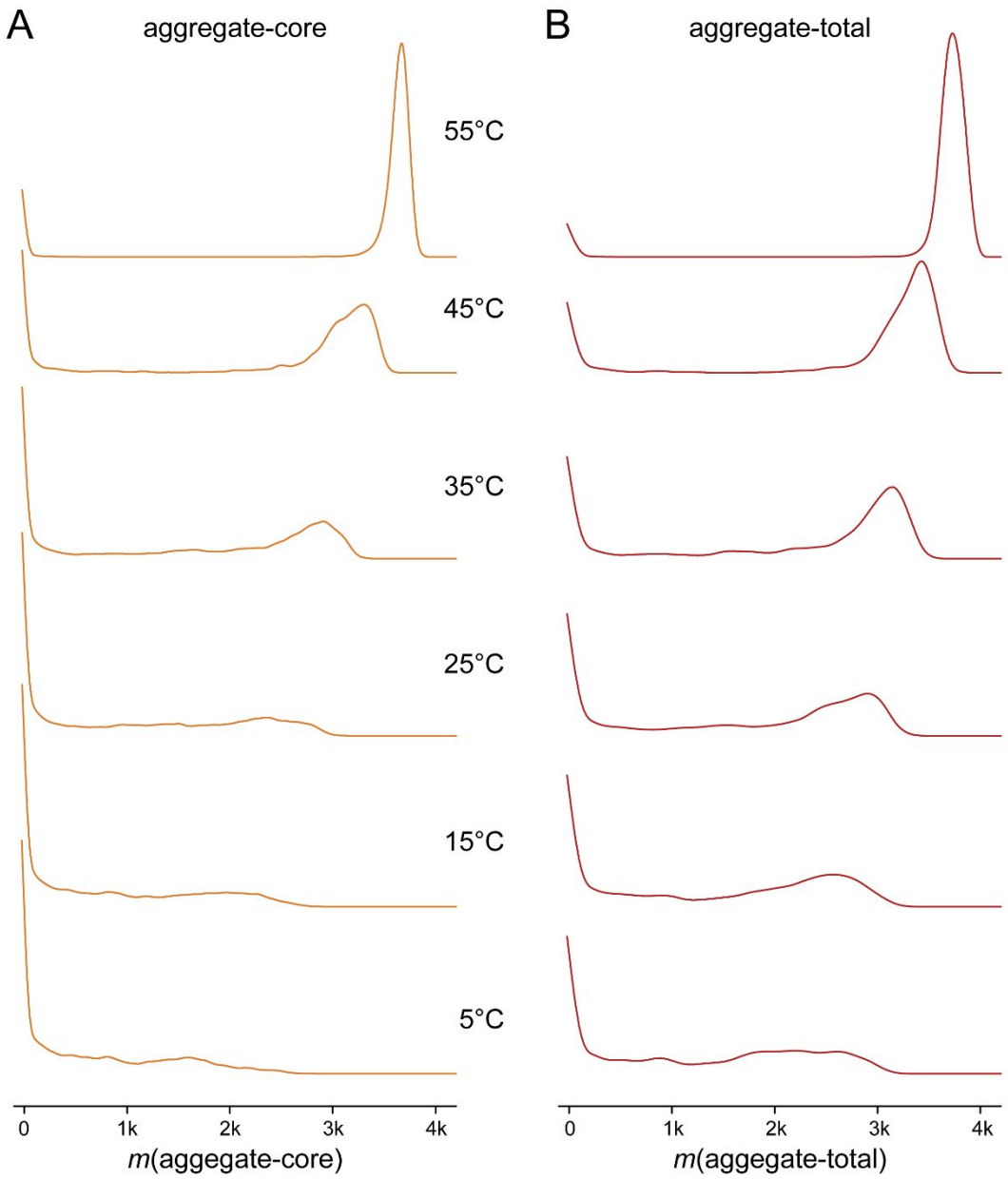

Figure S6. Aggregate size distribution at different temperatures. (A) Aggregate-core size distribution; (B) Aggregate-total size distribution. The very large aggregate at highest temperature refers to actually a precipitate. The T_{gel} and $T_{precipitate}$ in the system were about 30°C and 38°C, respectively. In this system, $Đ_M$(fixed M_w) = 2.2 and φ = 0.25. Chain models here were the default model chains.

S2.4 Micellar shape and network structure

In simulations, the shape of an aggregate-core was characterized by two parameters

—— area of aggregate-core ($S_{\text{aggregate-core}}$) and noncircularity ($\delta^*$), as schematically shown in Figure S7A.

The definition of $S_{\text{aggregate-core}}$ was

$$S_{\text{aggregate}-\text{core}} = \pi ab \tag{S1}$$

where a and b are the axial lengths of the equivalent ellipse of the aggregate-core, and can be calculated by the position matrix of all beads in the aggregate-core.

The δ^* was defined as follows:

$$\delta^* = 1 - 2\frac{a^2b^2 + b^2a^2}{(a^2 + b^2)^2} \tag{S2}$$

It varies from 0 (circle) to 1 (line). Therefore, a larger δ^* refers to a more heterogeneous structure (more like a line), while a smaller δ^* refers to a more homogeneous structure (more like a circle).

From Figure S7B, at low temperature, although the $S_{\text{aggregate-core}}$ increased with the decrease of $Đ_M$(fixed M_w) and with the increase of $Đ_M$(fixed M_n), the δ^* maintained a low value (< 0.4) in all polydispersed systems, indicating that the micellar shapes in all systems were close to circle.

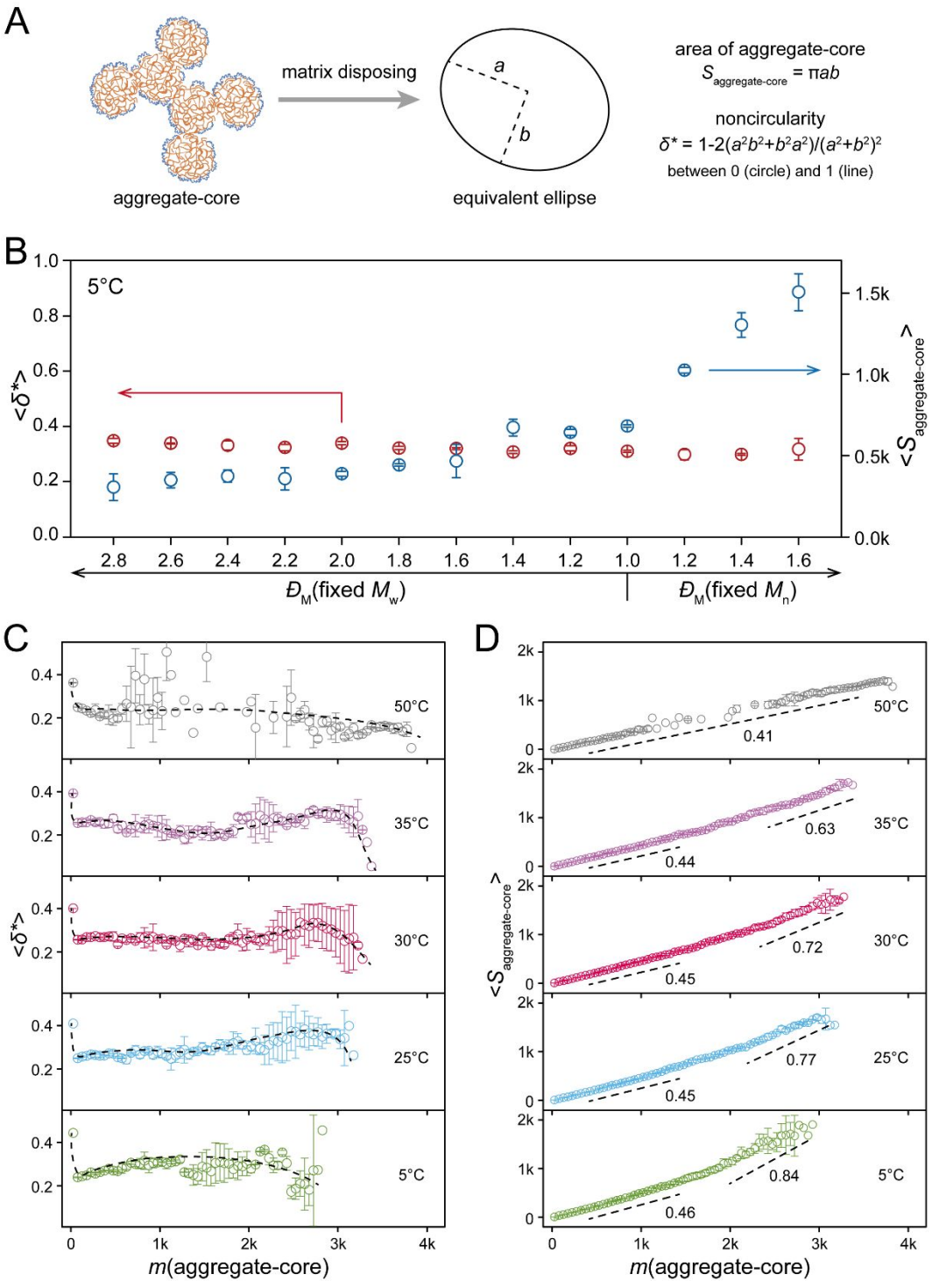

Figure S7. Structure of aggregate-cores in polydispersed systems. (A) Schematic of definitions of area of aggregate-core $S_{aggregate-core}$ and noncircularity δ^*; (B) δ^* and $S_{aggregate-core}$ in different polydispersed systems (φ = 0.25) at 5°C; (C-D) δ^* and $S_{aggregate-core}$ as a function of aggregate-core size $m_{aggregate-core}$ at different temperatures.

The number near the dashed line in (D) represents the slope of the line. In this system, $Đ_M$(fixed M_w) = 2.2 and φ = 0.25. Chain models here were the default model chains.

More detailed statistics about the shape of aggregate-cores are presented in Figures S7C and S7D. From Figure S7C, the high value of δ^* of small aggregate-cores (mainly isolated chains) indicated that these aggregate-cores were very heterogeneous (more like a line). Then, as $m_{\text{aggregate-core}}$ increased, the δ^* dramatically became smaller owing to the formation of the nearly circular micelle. At the range of high $m_{\text{aggregate-core}}$, the δ^* first increased but then decreased with $m_{\text{aggregate-core}}$. The increased δ^* corresponded to the heterogeneous aggregate of micelles, while the further decreased δ^* corresponded to the formation of some relatively homogeneous network-like structures. At low temperatures before thermogelation, the decreased tendency of δ^* at high $m_{\text{aggregate-core}}$ range was slight, but when the temperature was higher than T_{gel} (about 30°C in the system in Figure S7), this decreased tendency was more obvious. The decreased tendency further became slight when the temperature was higher than $T_{\text{precipitate}}$ (about 38°C in the system in Figure S7).

Results of $S_{\text{aggregate-core}}$ as a function of $m_{\text{aggregate-core}}$ are shown in Figure S7D. At temperatures lower than $T_{\text{precipitate}}$, the increase of $S_{\text{aggregate-core}}$ with $m_{\text{aggregate-core}}$ could be divided into two regions: a first slow increased region and a second fast increased region. The fast increased region indicated the loose large aggregate-cores, which might have a network-like structure. With the increase of temperature, the increased speed of the first region slightly decreased, indicating the collapse of the micelles; on the contrary, the increased speed of the second region decreased more obviously,

indicating the collapse of the network. At the temperature higher than $T_{\text{precipitate}}$, the increased tendency of $S_{\text{aggregate-core}}$ was uniform with $m_{\text{aggregate-core}}$ and the two different regions disappeared because of the formation of the dense precipitate.

S2.5 Evolution of hydrophobic channels and hydrophilic bridges as temperature increased

Both the hydrophobic channel and the hydrophilic bridge can act as the physical cross-linking points of the micellar network. We employed some parameters to demonstrate their roles in the thermogelling process.

Averaged number of micelle units of aggregates N_{micelle} was calculated by the following formula,

$$N_{\text{micelle}} = \frac{M_{\text{w}}(\text{aggregate})}{M_{\text{w}}(\text{aggregate} - \text{core}) \text{ at } 0℃} \quad \text{(S3)}$$

The micelle number in the aggregate-core and that in the aggregate-total can be determined using formulas similar to equation (S3).

From Figure S8A, the N_{micelle} of the aggregate-core increased with temperature, indicating that the micelles aggregated by the link of the hydrophobic channel. The N_{micelle} of the aggregate-total was larger than that of the aggregate-core at low temperatures, but at higher temperatures, these two parameters were very close. This implied that the formation of the hydrophobic channel was the key to the aggregation, while the hydrophilic bridge was relatively less important. From the direct statistics, the bridge fraction decreased as temperature increased (Figure S8B). Considering the definitions of the hydrophobic channel and the hydrophilic bridge, the decreased

bridge fraction was an inevitable result of the increase of the channel.

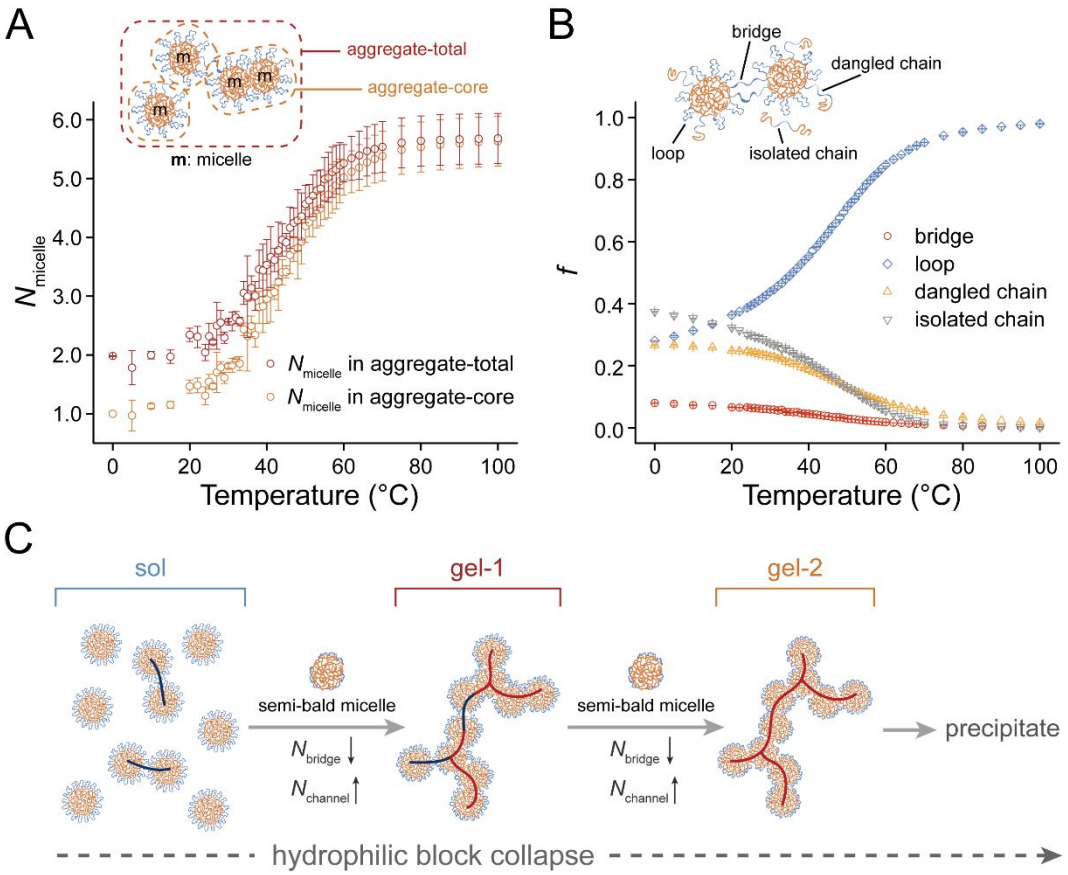

Figure S8. Roles of hydrophobic channels and hydrophilic bridges on thermogelation. (A) $N_{micelle}$ in aggregate as a function of temperature. The simulated chains in the polydispersed system ($Đ_M$(fixed M_w) = 2.2, φ = 0.25) were the default model chains; (B) Evolution of B block configurations with temperature. Data were collected from the same system with (A); (C) Schematic mechanism of the thermogelation process. Gel-1 and gel-2 are two thermogel substates with different extents of the main cross-linking points (hydrophilic bridge or hydrophobic channel). Here the red and blue curved lines represent micelles linked by hydrophobic channels and hydrophilic bridges, respectively.

Based on the results, the schematic mechanism of the thermogelation is presented in Figure S8C. In gel-1, the micelles in the percolated network are linked by both hydrophilic bridges and hydrophobic channels; in gel-2, in spite of the presence of a

low fraction of hydrophilic bridges, the skeleton of the percolated network is formed necessarily only by the hydrophobic channels among semi-bald micelles.

S2.6 Further confirmation of the $Đ_M$ effects on thermogelation

To further confirm the $Đ_M$ effects on thermogelation, we employed another set of chain models besides the default chain models. Three components in these polydispersed systems were $A_8B_{16}A_8$, $A_{24}B_{16}A_{24}$, and $A_{40}B_{16}A_{40}$, where $A_{24}B_{16}A_{24}$ was the starting point for changing $Đ_M$. From Figure S9, similar to the results from the default systems (Figure 4), a non-monotonic tendency of T_{gel} with the increase of MW (either M_w or M_n) was observed in the above polydispersed systems. But for the corresponding monodispersed systems, the tendency was monotonic. These results further confirmed that $Đ_M$ was a molecular parameter independent of molecular weight to affect the thermogelling behavior.

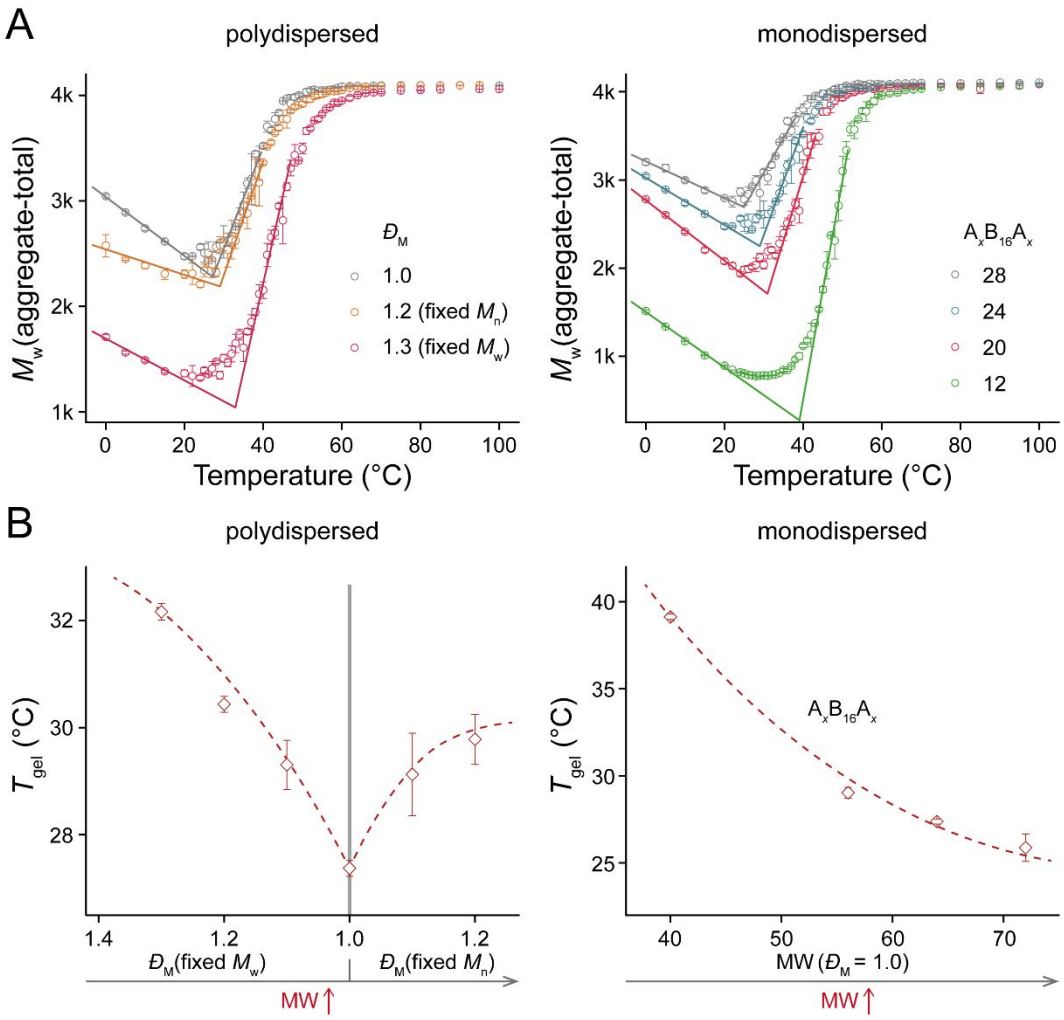

Figure S9. Further confirmation of the $Đ_M$ effects on thermogelation. (A) M_w(aggregate-total)-T curves of the indicated systems. Three components in the polydispersed systems here were $A_8B_{16}A_8$, $A_{24}B_{16}A_{24}$, and $A_{40}B_{16}A_{40}$; (B) Evolution of T_{gel} against $Đ_M$ or MW of indicated systems. For all systems, φ = 0.25.

S2.7 Micellar structures at low temperatures before thermogelation

The above results illustrate that $Đ_M$ is an independent parameter to modulate thermogelling behaviors. Because micelles are the precursor of the hydrogel network, we speculate that the micellar structure might be affected by the $Đ_M$. A series of quantities were calculated to characterize the micellar morphology.

Gyration radii of the aggregate-core (with both blocks A and B) and the core in this aggregate-core (with only block A joining in statistics) were calculated by

$$R_{\mathrm{g}} = (R_{\mathrm{g}}^{\,2})^{0.5} = \left(\frac{\sum m_i \boldsymbol{r}_i^{\,2}}{\sum m_i}\right)^{0.5} \tag{S4}$$

where m_i represents the mass of the i-th bead in an aggregate, and is equal to 1 for all beads; $\boldsymbol{r}_i$ is the position vector from the i-th bead to the centroid of the aggregate. From Figure S10, both the R_{g}(aggregate-core) and R_{g}(core) increased with the decrease of $Đ_{\mathrm{M}}$(fixed M_{w}) and with the increase of $Đ_{\mathrm{M}}$(fixed M_{n}).

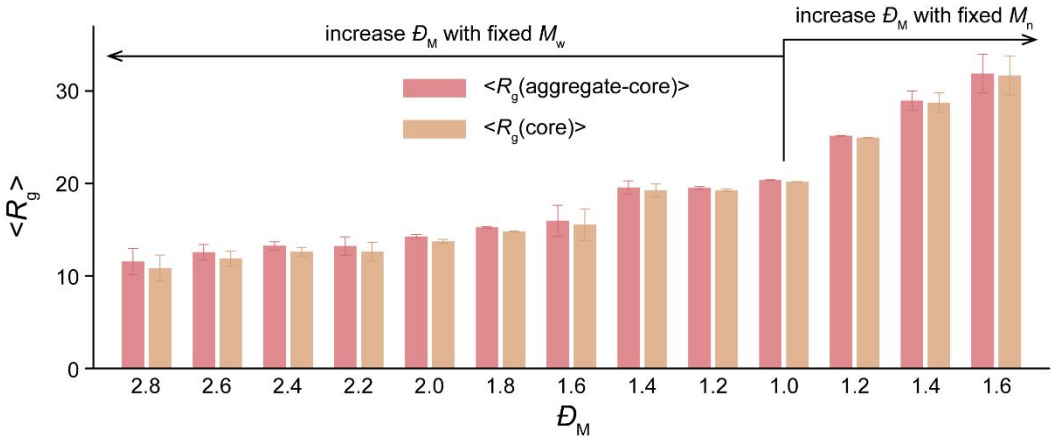

Figure S10. R_{g}(aggregate-core) and R_{g}(core) in indicated systems at 5°C. Chain models in polydispersed systems (φ = 0.25) were the default model chains.

Then, we employed R_{g}(central bead) or R_{g}(linking bead) to characterize the apparent radii of the aggregate-core or the core. The definition of these two parameters were similar to the R_{g}(aggregate-core) and R_{g}(core), but only the central bead and the linking bead of the ABA model chain were considered. In statistics, an ABA model chain was also considered as two AB semi-chains. As schematically shown in Figure S11, the apparent radius can reflect the contour size of the aggregate.

The changing tendencies of these two parameters (Figure S11) were similar to those of R_g(aggregate-core) and R_g(core) in Figure S10.

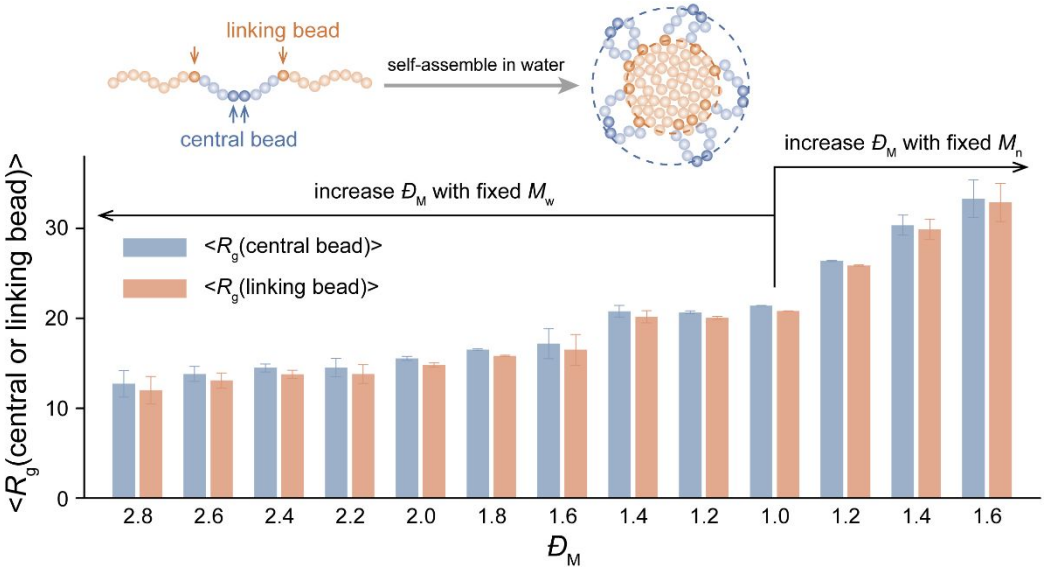

Figure S11. Apparent radius of micelle or core in the indicated systems at 5°C. Chain models in polydispersed systems (φ = 0.25) were the default model chains.

In simulations, the definition of the corona thickness d_{corona} is

$$d_{\text{corona}} = R_g(\text{aggregate} - \text{core}) - R_g(\text{core}) \quad \text{(S5)}$$

Figure S12 illustrated that the increase of $Đ_M$ led to relative thickening of the micellar coronae irrespective of fixing M_n or M_w.

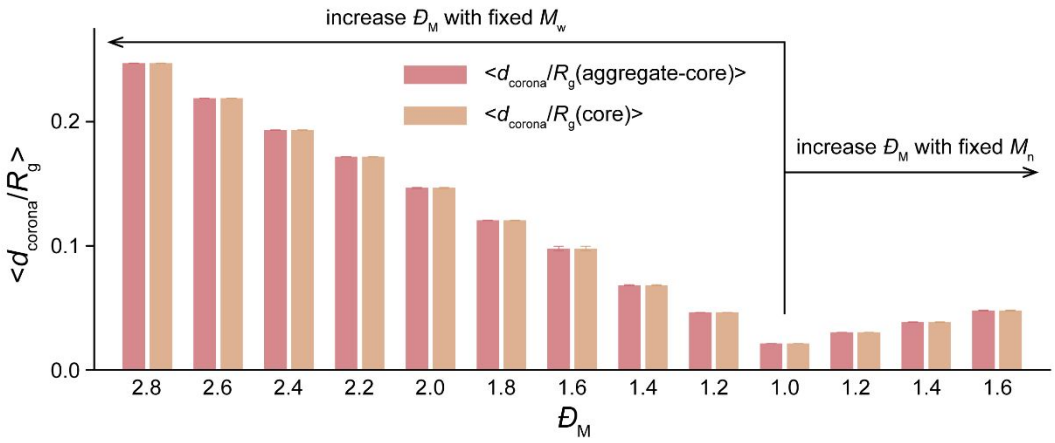

Figure S12. Ratios of the d_{corona} and R_g(aggregate-core) or R_g(core) in indicated systems at 5°C. Chain models in polydispersed systems (φ = 0.25) were the default model chains.

The roughness of the micellar core was defined as follows:

$$\text{Roughness} = \frac{1}{n}\sum_{i=1}^{n}|r_i - \bar{r}| \quad \text{(S6)}$$

Here, the n is the number of AB semi-chains in the corresponding aggregate-core; the r_i is the distance between the i-th linking bead and the centroid of the core; and the $\bar{r}$ is the average distance from all linking beads to the centroid of the core. From Figure S13, the roughness of the micellar core increased with the decrease of $Đ_M$(fixed M_w) and with the increase of $Đ_M$(fixed M_n).

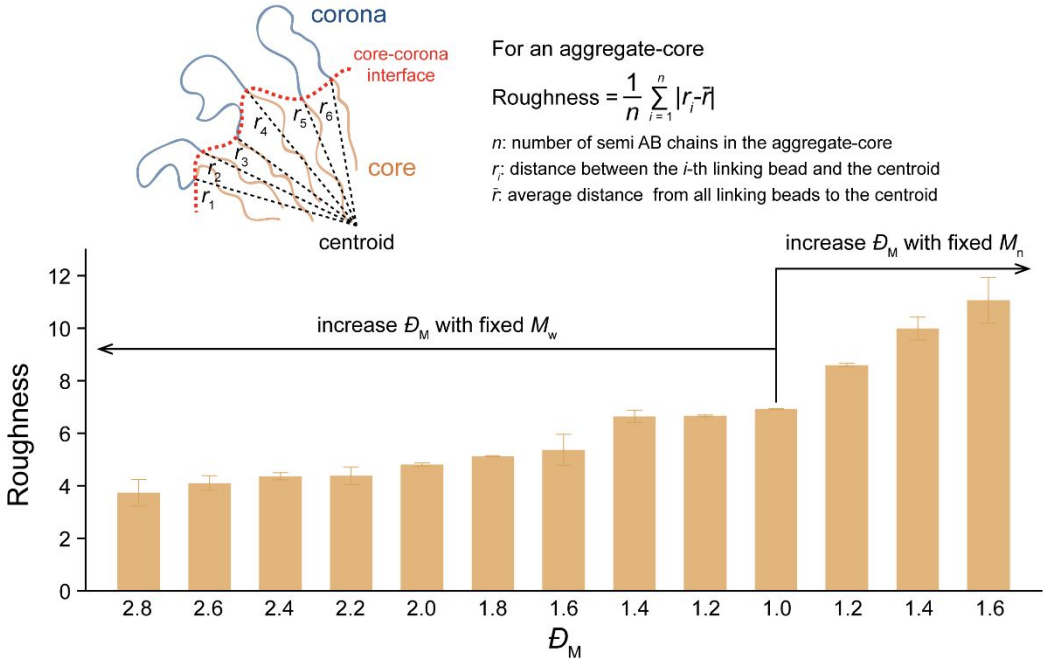

Figure S13. Roughness of micellar cores in indicated systems at 5°C. Chain models in polydispersed systems (φ = 0.25) were the default model chains.

The properties of the core-corona interface can also be reflected by the pairwise AB contact. From Figure S14. This parameter decreased with the decrease of $Đ_M$(fixed M_w) and with the increase of $Đ_M$(fixed M_n).

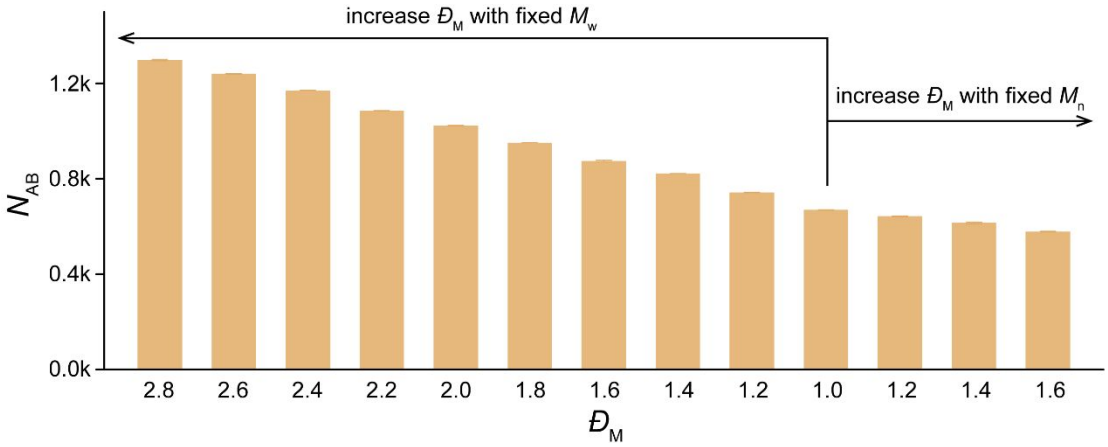

Figure S14. Pairwise AB contact in indicated systems at 5°C. Chain models in polydispersed systems (φ = 0.25) were the default model chains.

S2.8 Further confirmation of the relationship between T_{gel} and d_{corona}

Besides the default chain models, another set of chain models, $A_8B_{16}A_8$, $A_{24}B_{16}A_{24}$, and $A_{40}B_{16}A_{40}$, was also modelled to confirm the relationship between T_{gel} and d_{corona}. From Figure S15, in the same path of modulating $Đ_M$ ($Đ_M$(fixed M_w) or $Đ_M$(fixed M_n)), a significant correlation between d_{corona} and T_{gel} was observed. The relation between these two parameters was also observed in the corresponding monodispersed systems. These results further confirmed the relevance between T_{gel} and d_{corona}.

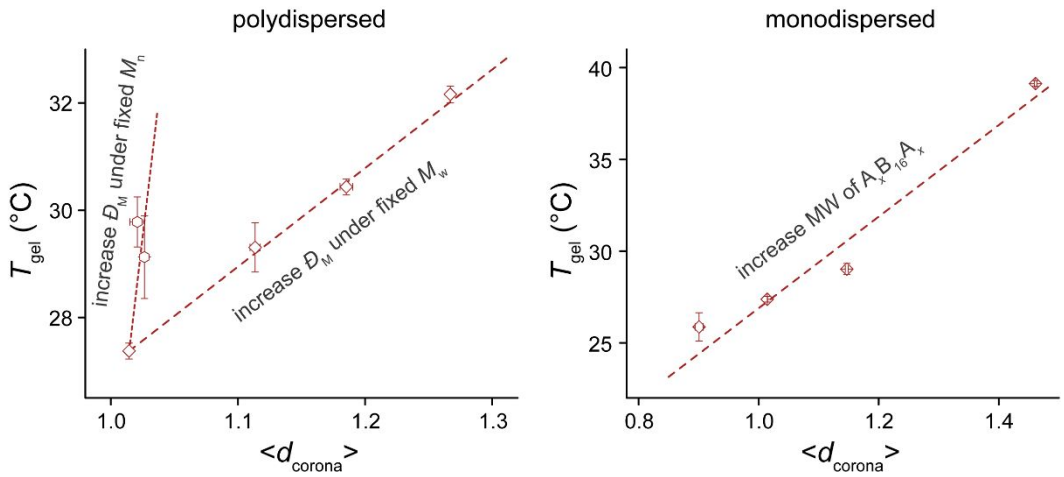

Figure S15. T_{gel} as a function of d_{corona} in unit of lattice size in the indicated simulation systems. Three components in the polydispersed systems were $A_8B_{16}A_8$, $A_{24}B_{16}A_{24}$, and $A_{40}B_{16}A_{40}$. The system parameters here were the same as those in Figure S9.

S2.9 Heterogeneous spatial distribution of different chains in an aggregate

Assembly structures of micelles at low temperatures before thermogelation were analyzed in detail. The normalized density profiles of different beads along the micelle radius are shown in Figure S16. We found that the spatial distribution of different chains in a micelle was heterogeneous. The P1, P2, and P3 preferred to distribute from outside to inside along the micellar radius.

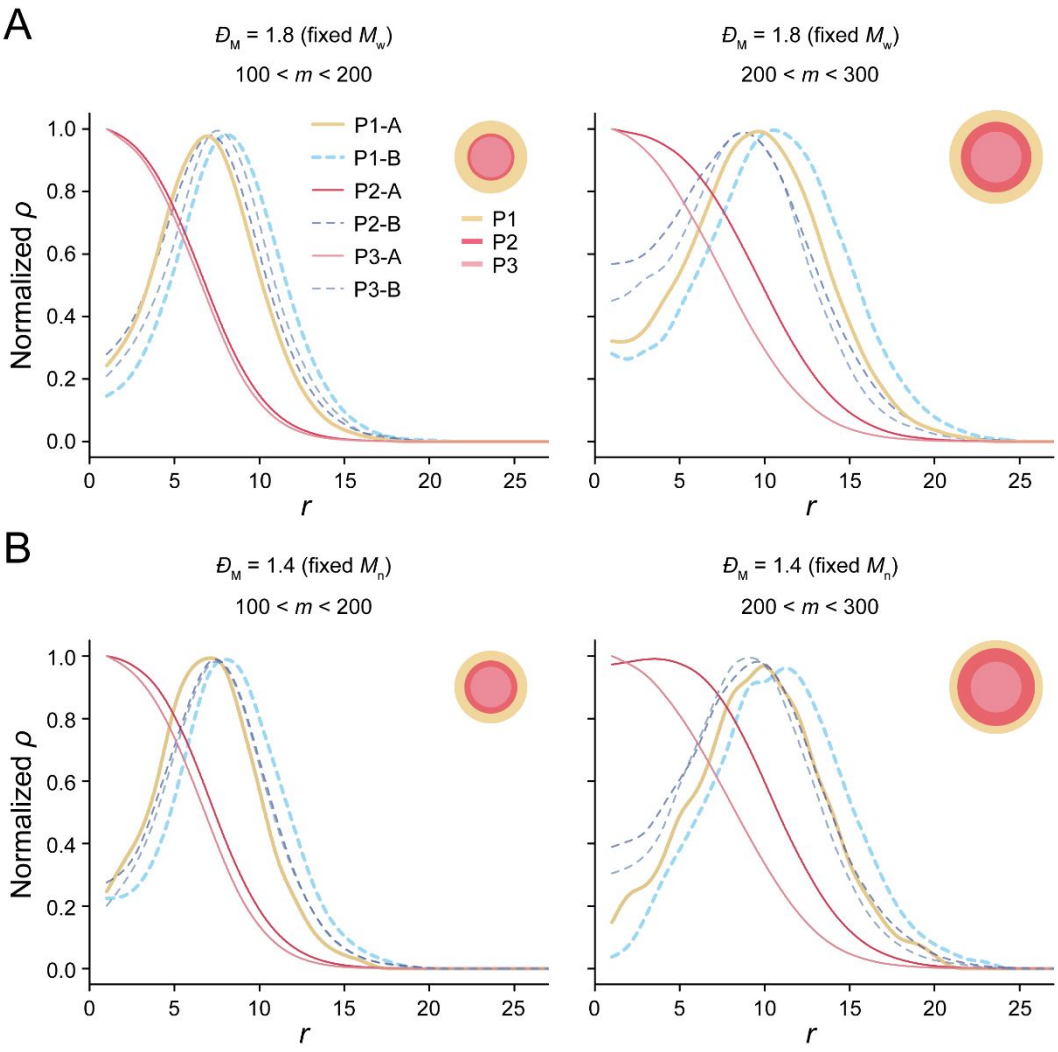

Figure S16. Heterogeneous spatial distribution of different components in aggregates at a low temperature (5°C). Normalized density profiles of different beads (normalized by the maximum) in aggregates with indicated sizes were calculated. (A) Data from the system with $Đ_M$(fixed M_w) = 1.8 and φ = 0.25; (B) Data from the system with $Đ_M$(fixed M_n) = 1.4 and φ = 0.25. Here, m represents the mass of the aggregate-core. Chain models here were the default model chains.

To obtain more quantitative understanding, the relative position of the Pi component to the core-corona interface was defined and calculated by

$$\Delta r(\mathrm{P}i) = \frac{1}{n_{\mathrm{P}i}} \sum_{j=1}^{n_{\mathrm{P}i}} (r_j - \bar{r}) \qquad \text{(S7)}$$

where $n_{\mathrm{P}i}$ represents the number of semi Pi chains in the aggregate-core; r_j is the

distance between the *j*-th linking bead of semi P*i* chains and the centroid of the core; and $\bar{r}$ is the average distance from all linking beads of all components to the centroid of the core.

From Figure S17, the relatively more hydrophilic P1 component preferred to be located at the outside of the interface, and the more hydrophobic P3 component exhibited opposite preference.

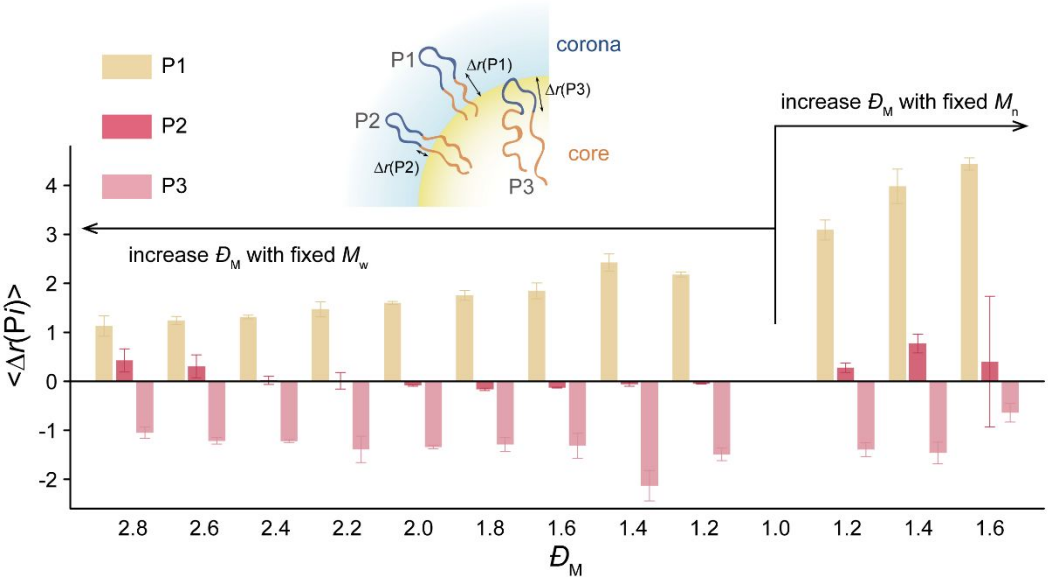

Figure S17. Position of different chains in aggregate-cores at 5°C. Chain models in polydispersed systems (φ = 0.25) were the default model chains.

Further analysis was conducted by the statistics of the solvent coordination number of different beads. If a bead prefers to be located at the outside of the aggregate, the coordination number is larger. Results from Figure S18 indicated that the intra-micelle heterogeneity maintained even after thermogelation and got to be insignificant at the precipitate state.

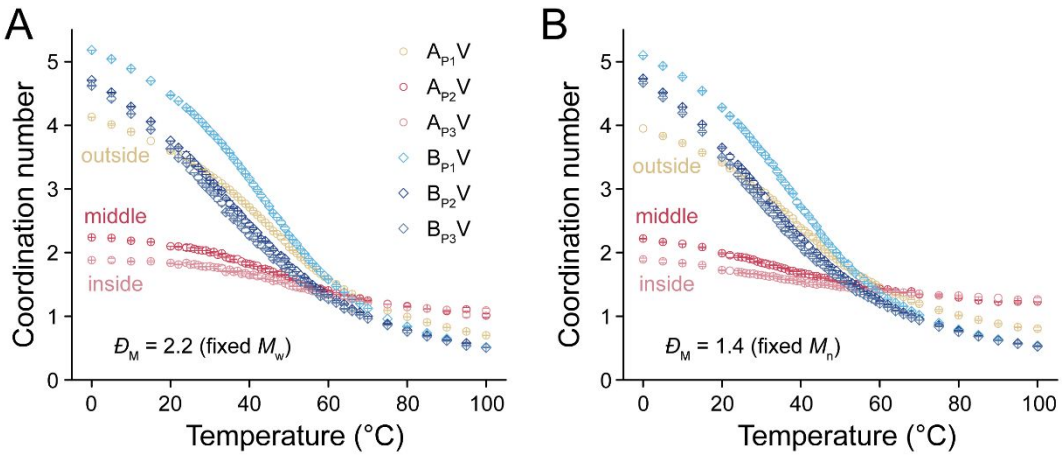

Figure S18. Evolution of the heterogeneous distribution of different chains in aggregates with temperature. Solvent coordination numbers of the indicated bead types were calculated. $A_{Pi}V$ and $B_{Pi}V$ represent the solvent (V) coordination numbers of the A and B beads of the P*i* chain, respectively. (A) Data from the system with $Đ_M$ = 2.2 (fixed M_w) and φ = 0.25; (B) Data from the system with $Đ_M$ = 1.4 (fixed M_n) and φ = 0.25. The simulated chains here were the default model chains.

S2.10 Contributions of different chains to corona thickness

The contribution of each type of chain to the corona thickness was characterized by d_{corona}(P*i*). The d_{corona}(P*i*) of a micelle was defined as

$$d_{\text{corona}}(\text{P}i) = \frac{\sum_{j=1}^{n_{\text{P}i}} d_j(\text{P}i)}{n_{\text{P}i}} = \frac{\sum_{j=1}^{n_{\text{P}i}} (r_j(\text{central bead of P}i) - r_j(\text{linking bead of P}i))}{n_{\text{P}i}} \quad \text{(S8)}$$

Here, the r_j(central bead of P*i*) represents the distance between the *j*-th central bead of P*i* chains in the micelle and the micellar centroid; the r_j(linking bead of P*i*) represents the distance between the *j*-th linking bead of P*i* chains in the micelle and the micellar centroid; the n_{Pi} is the number of the semi P*i* chain in the micelle.

The statistics results of d_{corona}(P1), d_{corona}(P2) and d_{corona}(P3) are summarized in Figure S19. The tendency of the d_{corona}(P1) with $Đ_M$ was similar to the tendency of the d_{corona} with $Đ_M$ (Figure 5B), indicating that the P1 component might make a larger

contribution to the corona thickness.

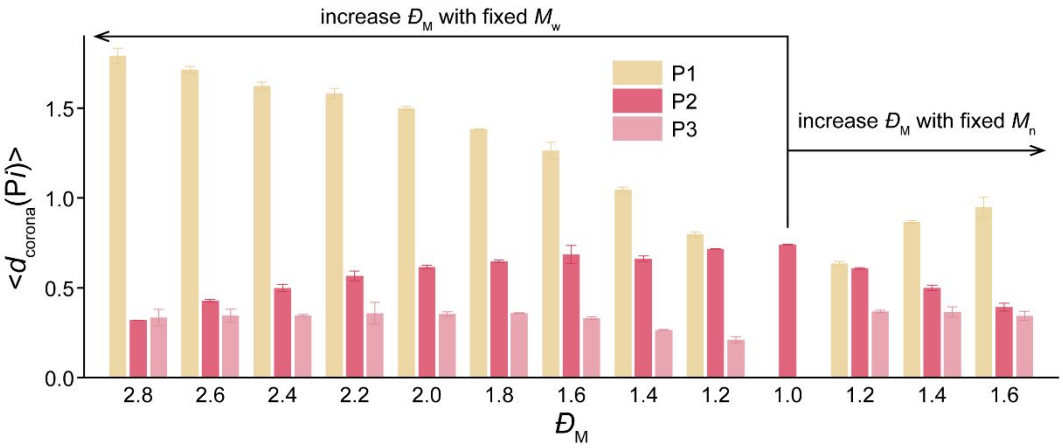

Figure S19. Contributions of different chains to corona thickness in indicated systems (φ = 0.25) at 5°C. Chain models here were the default model chains.

S2.11 Roles of different chains on thermogelation

M_w(P*i*P*j*) was employed to characterize the aggregation of every two types of chains P*i* and P*j* in polydispersed systems. This parameter was similar to the M_w(aggregate-core), but only two components P*i* and P*j* were considered in statistics while all of the three components (P1, P2, and P3) were simulated. The results are shown in Figure S20. Then M_w(P*i*) was calculated to evaluate the self-aggregation of each component. Normalized M_w(P*i*) by the M_w(P*i*) at 0°C was further analyzed. From this analysis, the roles of P2 and P3 in thermogelation were revealed. The hydrogel network skeleton was constituted mainly by P2 and P3. P2 acted as the skeleton adhesive and P3 acted as the skeleton unit.

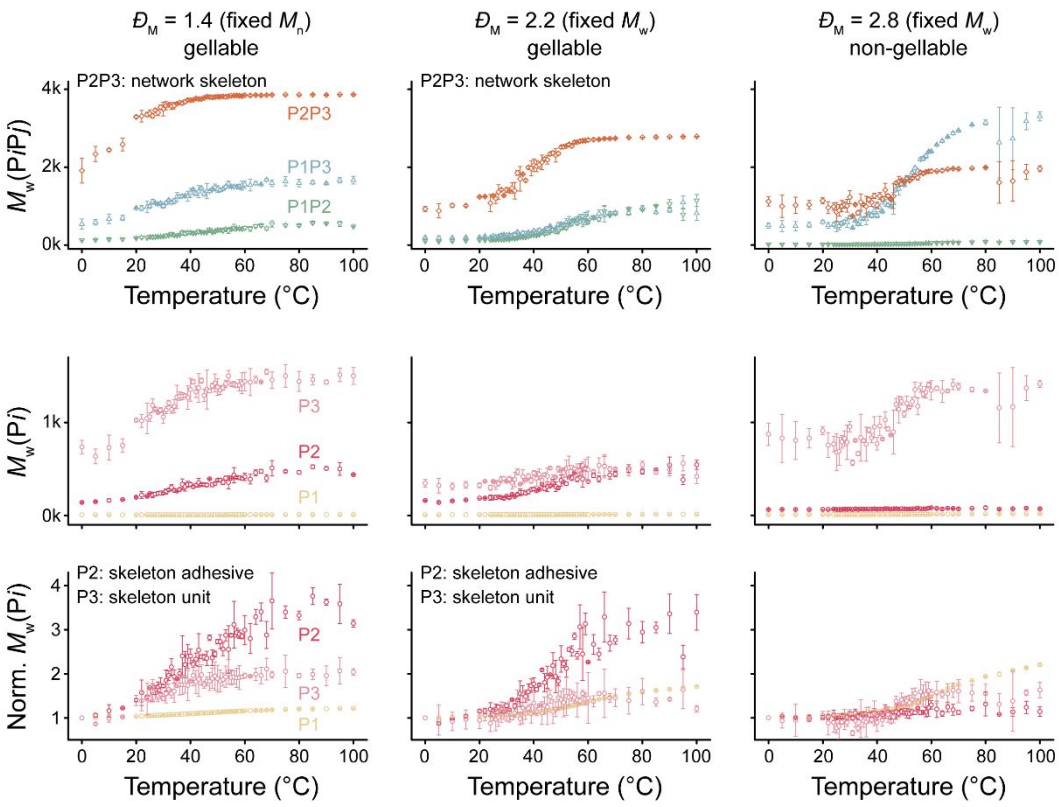

Figure S20. Roles of medium MW and high MW chains playing in the thermogelling process. (Upper row) M_w(P*i*P*j*) as a function of temperature in the indicated systems; (Middle and lower rows) M_w(P*i*) and normalized M_w(P*i*) as a function of temperature in the indicated systems. P1, P2, and P3 represent the low MW ($A_2B_8A_2$), medium MW ($A_{28}B_8A_{28}$), and high MW ($A_{54}B_8A_{54}$) chains, respectively. The φ values of all systems were 0.25.

The roles of different chains in thermogelation were further investigated by comparing the polydispersed system (containing P1, P2, and P3) with the "knock-out" system of only two components, namely, lacking P*i*. The "knock-out" system lacked P*i* component but the other two components in the system were the same as those in the corresponding polydispersed system. The values of M_w(aggregate-core) of these systems are shown in Figure S21, which further reveals the role of P1 in thermogelation. The P1 hindered the aggregation of the system and acted as a micellar

stabilizer. In addition, the conclusions of the roles of P2 and P3 in thermogelation can also be strengthened by these results.

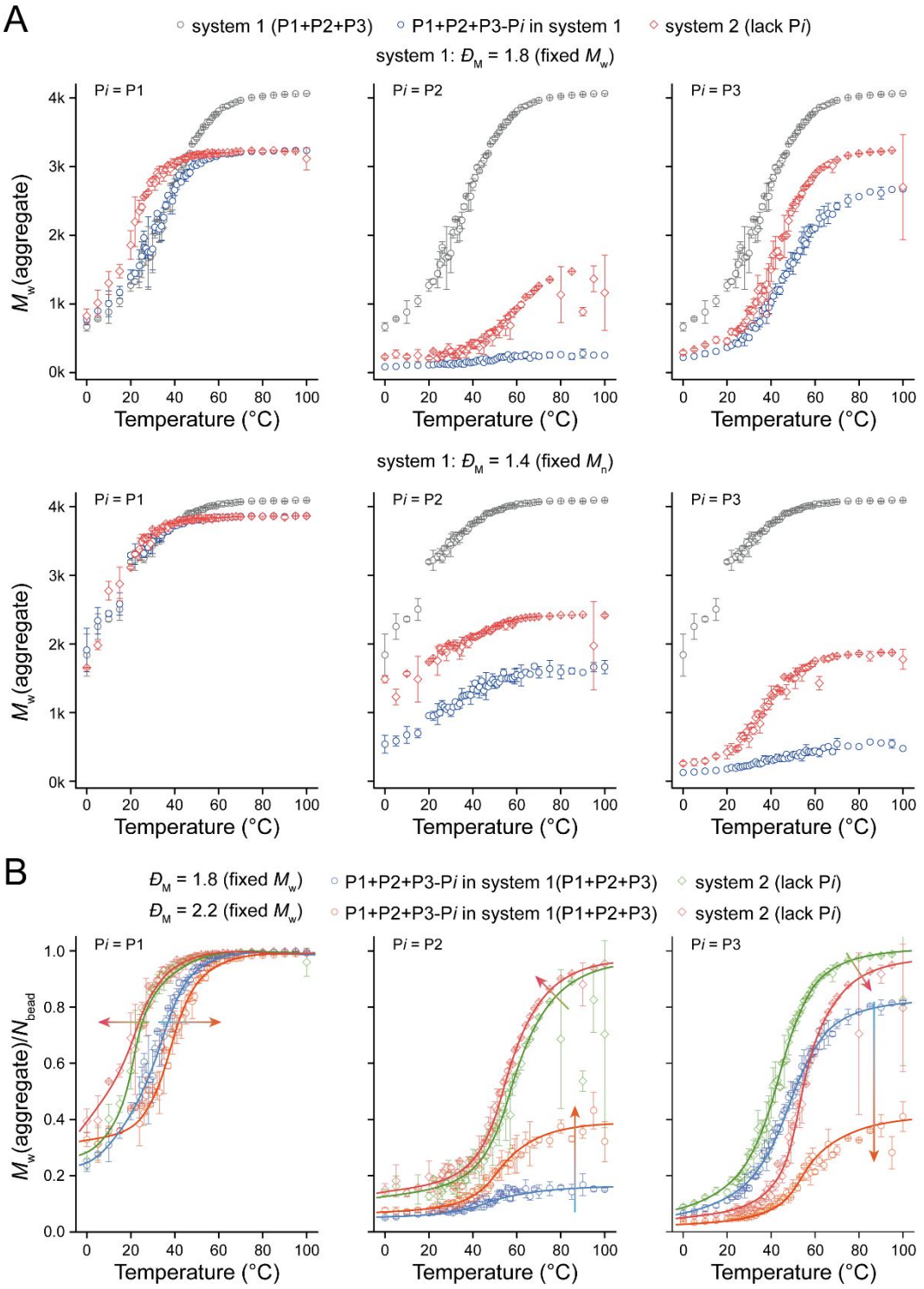

Figure S21. Roles of different MW components on thermogelation. (A) Evolutions of M_w(aggregate) with the increase of temperature in the indicated systems. System 1 contained P1, P2, and P3 components. System 2 contained only two components,

namely, the components in system 2 were the same as the components except P*i* in system 1. In order to illustrate the roles of different components on thermogelation more clearly, the M_w(aggregate) of the components except P*i* in system 1 (marked as "P1+P2+P3-P*i* in system 1" in the figure) was also calculated (here, three components were simulated together, but only two components joined in statistics) to compare with the aggregation of the system 2 with only two components, because both groups (P1+P2+P3-P*i* in system 1 and system 2) contain the same species; (B) Evolution of M_w(aggregate)/N_{bead} against temperature in the indicated systems. The arrows indicate the change tendency of the corresponding parameter from low $Đ_M$ ($Đ_M$(fixed M_w) =1.8) to high $Đ_M$ ($Đ_M$(fixed M_w) = 2.2). For all systems, φ = 0.25.

S2.12 Evolution of the distribution of each component in aggregates as temperature increased

We also carried out statistics of distribution of each component in different aggregates. According to Figure S22, P1 inclined to be isolated chains or enter into small micelles. As temperature increased, the fraction of the isolated P1 chains decreased, while the fraction of the P1 in larger aggregates increased. The fractions of P2 and P3 in larger micelles were high even at low temperatures and increased upon heating.

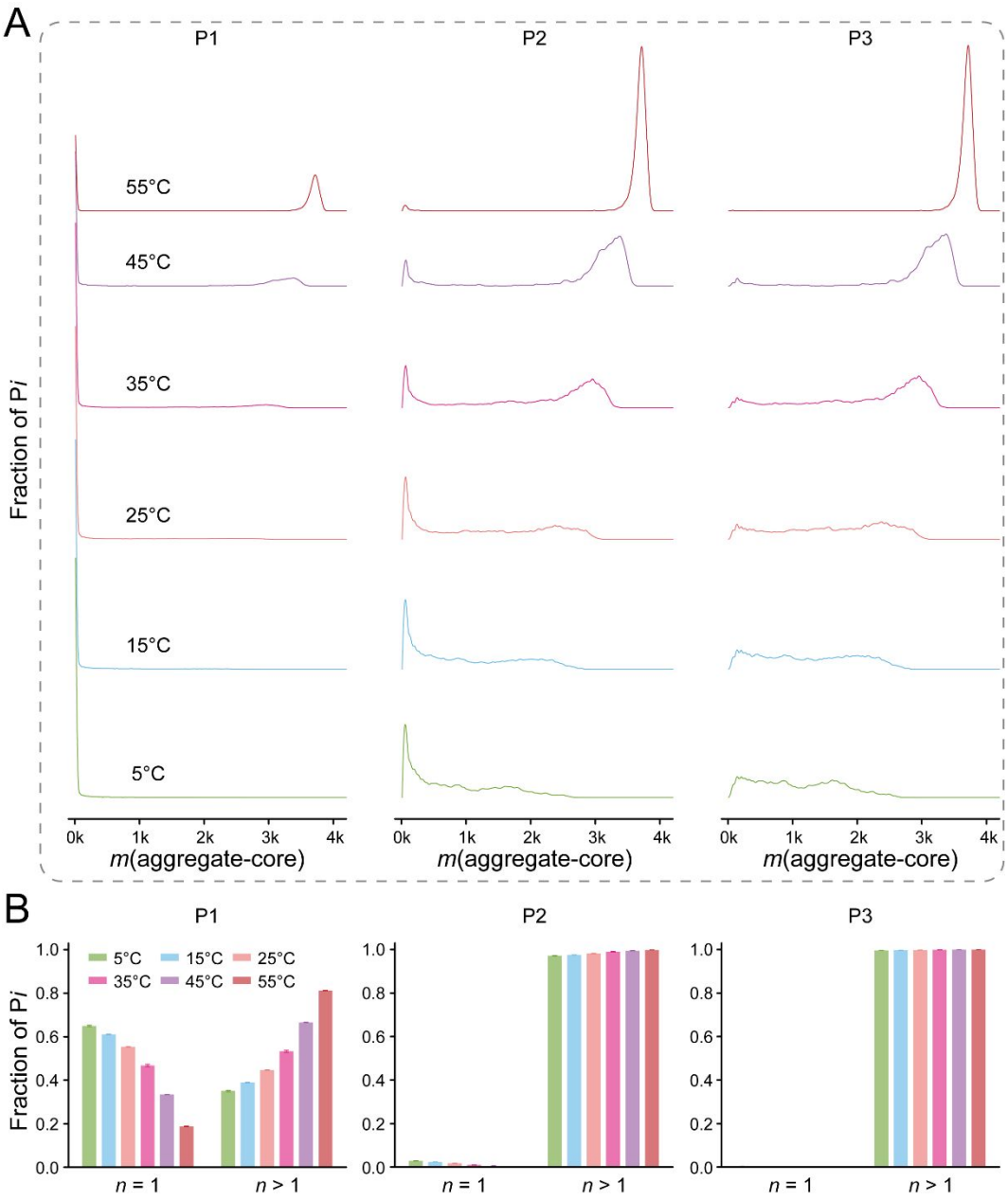

Figure S22. Evolution of component distribution in aggregates as temperature increased. (A) Weight distributions of different components in aggregates in the system with $Đ_M$(fixed M_w) = 2.2 and φ = 0.25. The T_{gel} and $T_{precipitate}$ in this system were around 30°C and 38°C, respectively; (B) Fraction of P*i* as isolated chains (n = 1) or in an aggregate-core with n > 1. Here, n represents the number of semi-chains in an aggregate-core. The φ of the system ($Đ_M$(fixed M_w) = 2.2) was 0.25. Chain models here were the default model chains.

S2.13 Small micelles in different systems at low temperature

The numbers of isolated chains and small micelles ($m_{\text{aggregate-core}} < 100$) in different systems at low temperature were counted. As presented in Figure S23, the number of the small micelles increased with $Đ_M$ (either $Đ_M$(fixed M_w) or $Đ_M$(fixed M_n)).

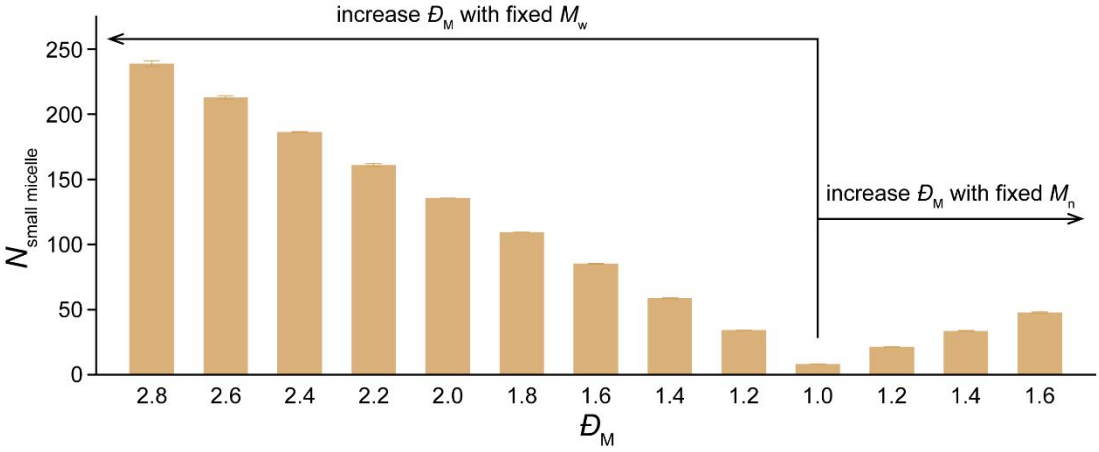

Figure S23. Number of small micelles ($m_{\text{aggregate-core}} < 100$) in different systems at 5°C. Chain models in polydispersed systems (φ = 0.25) were the default model chains.

S2.14 Volume fraction of aggregate-core in different systems at low temperatures

Volume fraction of aggregate-core Φ was calculated by

$$\emptyset = \frac{\sum_{i=1}^{n} S_i(\text{aggregate} - \text{core})}{L^2} \tag{S9}$$

where n is the number of aggregate-cores in the system, S_i(aggregate-core) is the area of the i-th aggregate-core, and can be obtained from equation (S1); and L^2 is the lattice number.

From Figure S24, the Φ decreased as $Đ_M$ (either $Đ_M$(fixed M_w) or $Đ_M$(fixed M_n)) increased, which might be ascribed to the increase of the isolated chains or small micelles with small volumes in more polydispersed systems.

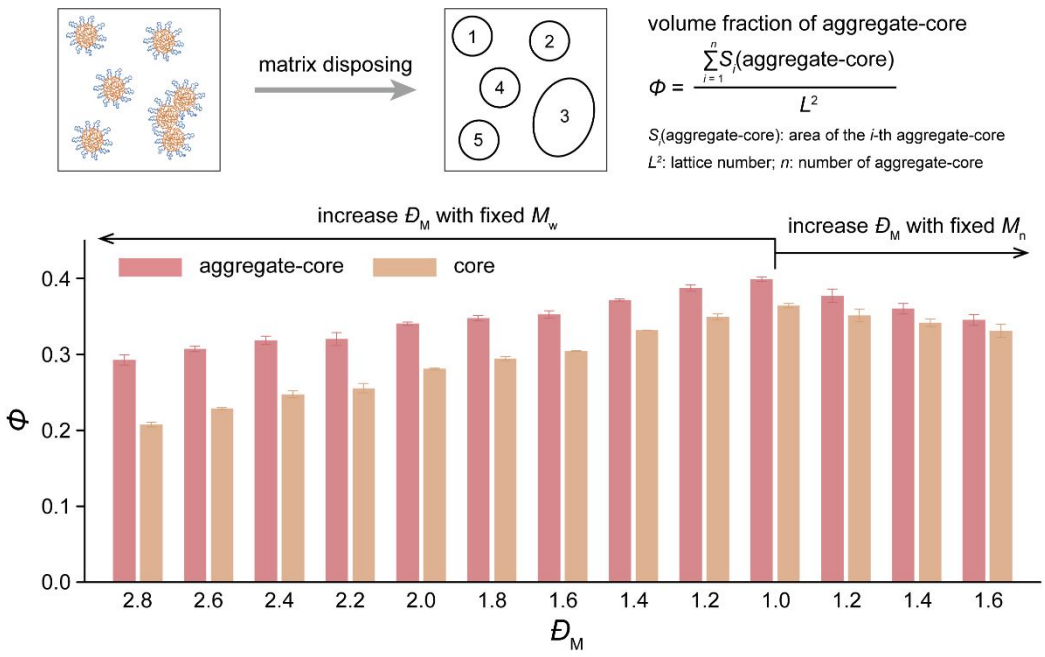

Figure S24. Volume fraction of micelles in different systems at 5°C. Chain models in polydispersed systems (φ = 0.25) were the default model chains.

S2.15 Evolution of the fractions of the components in aggregates as temperature increased

Fractions of different components over all components in aggregates with different sizes are shown in Figure S25. As temperature increased, the fraction of P1 in large micelles increased, indicating the fusion of the isolated P1 chains to the larger micelles.

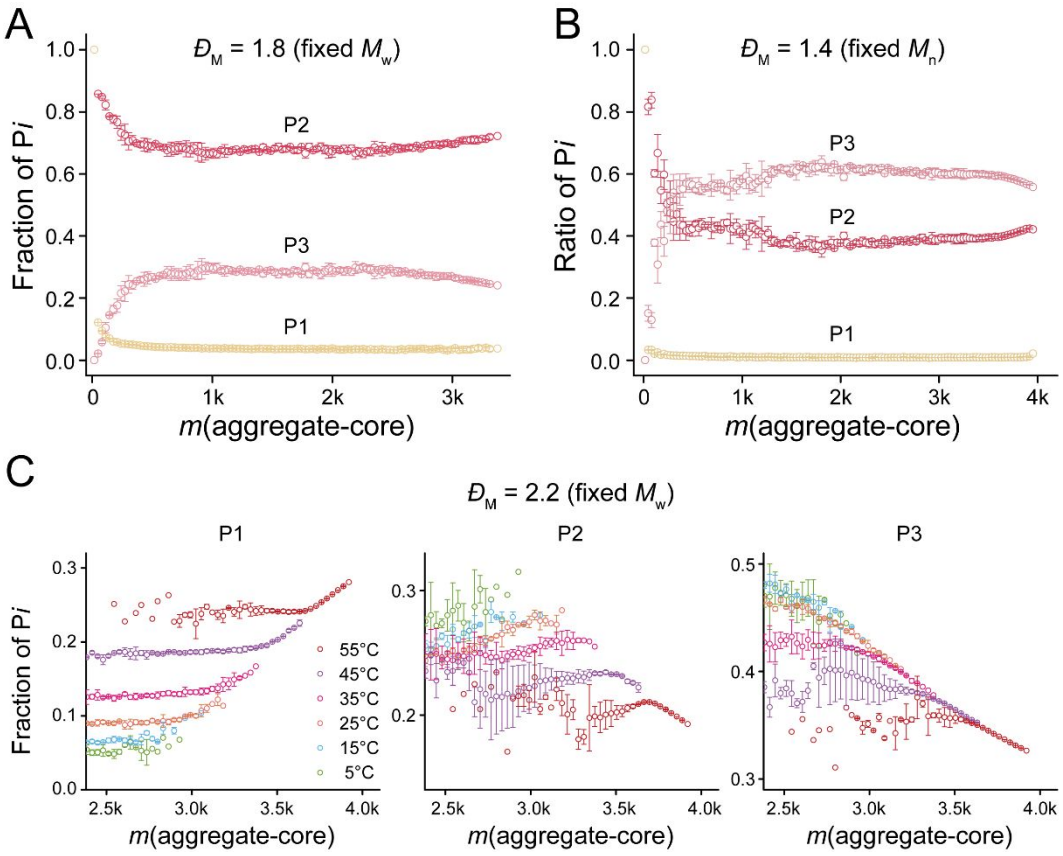

Figure S25. Weight fractions of different components in aggregates in the indicated systems under φ = 0.25 and varied MWD and temperature. The temperature of systems in (A) and (B) was 5°C. Chain models here were the default model chains.

This fusion from isolated chains or smaller micelles mainly with P1 to larger micelles might be attributed to the different corona thickness of different micelles (Figure S26). The coronae of larger micelles were much thinner, and thus the larger micelles got to be unstable. Then in order to stabilize these unstable micelles, the isolated chains or small micelles mainly with P1 had to fuse to the larger micelles. These results further reflected that the P1 acted as a micellar stabilizer.

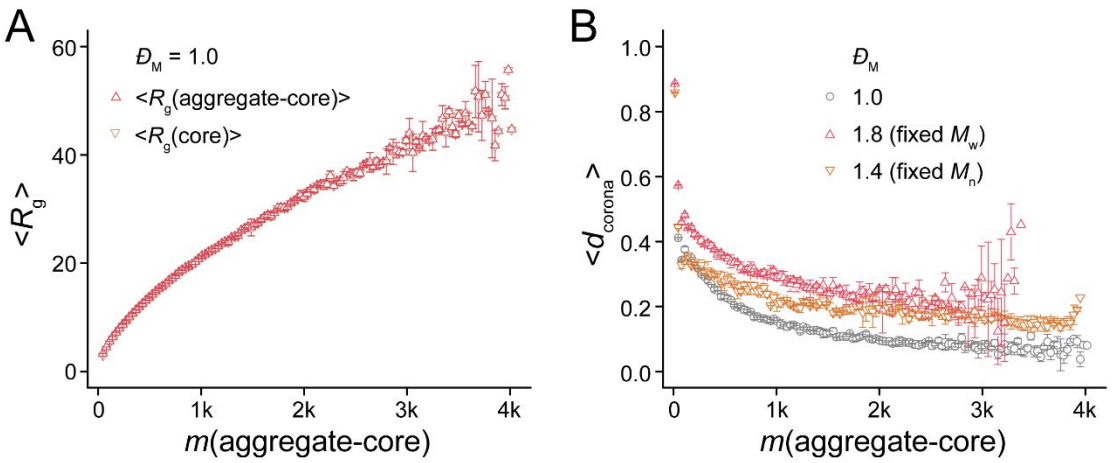

Figure S26. Structures of micelles with different sizes in indicated systems at 5°C. (A) R_g(aggregate-core) and R_g(core) as a function of mass of aggregate-core m(aggregate-core); (B) d_{corona} as a function of m(aggregate-core). The simulated chains here were the default model chains. The φ of all systems was 0.25.

S2.16 Effects of $Đ_M$ from hydrophilic blocks and hydrophobic blocks on micellar coronae

We also compared the effects of $Đ_M$ from hydrophobic blocks and hydrophilic blocks on corona thickness. The results are shown in Figure S27. In systems with dispersed hydrophilic blocks, the effect of $Đ_M$(fixed M_n) on corona thickness was more obvious than that of $Đ_M$(fixed M_w); while systems with dispersed hydrophobic blocks exhibited the opposite trend.

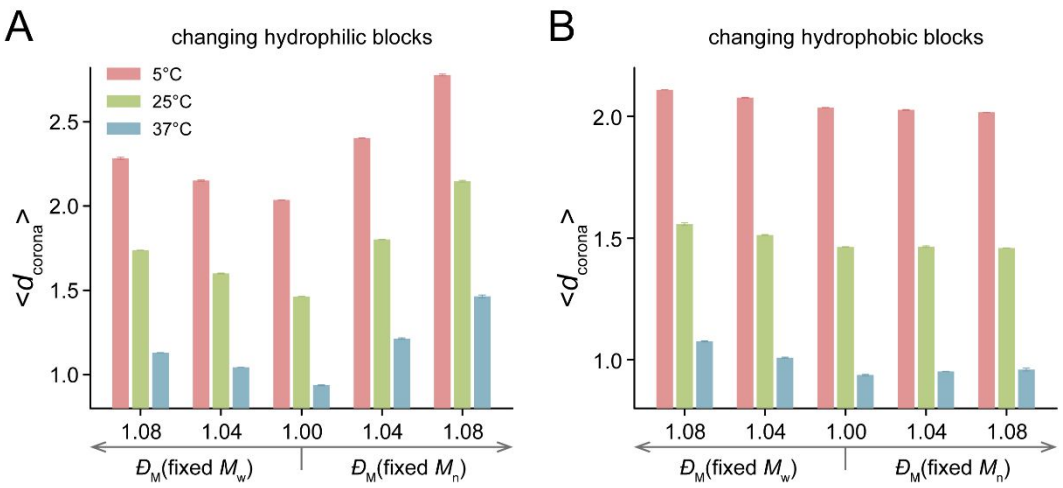

Figure S27. Corona thickness d_{corona} of the indicated systems at different temperatures. (A) Data from systems with modulating $Đ_M$ by changing hydrophilic blocks. Three components in the system were $A_{20}B_4A_{20}$, $A_{20}B_{24}A_{20}$, and $A_{20}B_{44}A_{20}$, where $A_{20}B_{24}A_{20}$ was the starting point for changing $Đ_M$; (B) Data from systems with modulating $Đ_M$ by changing hydrophobic blocks. Three components in the system were $A_{10}B_{24}A_{10}$, $A_{20}B_{24}A_{20}$, and $A_{30}B_{24}A_{30}$, where $A_{20}B_{24}A_{20}$ was the starting point for changing $Đ_M$. For all systems, $\varphi = 0.25$.

S2.17 Micelle size and bridge fraction of systems with dispersed hydrophilic blocks at low temperatures

Micelle size and bridge fraction of systems with $Đ_M$ from hydrophilic blocks at low temperatures were calculated. The results are shown in Figure S28. As either $Đ_M$(fixed M_w) or $Đ_M$(fixed M_n) increased, the micelle size increased and the bridge fraction decreased.

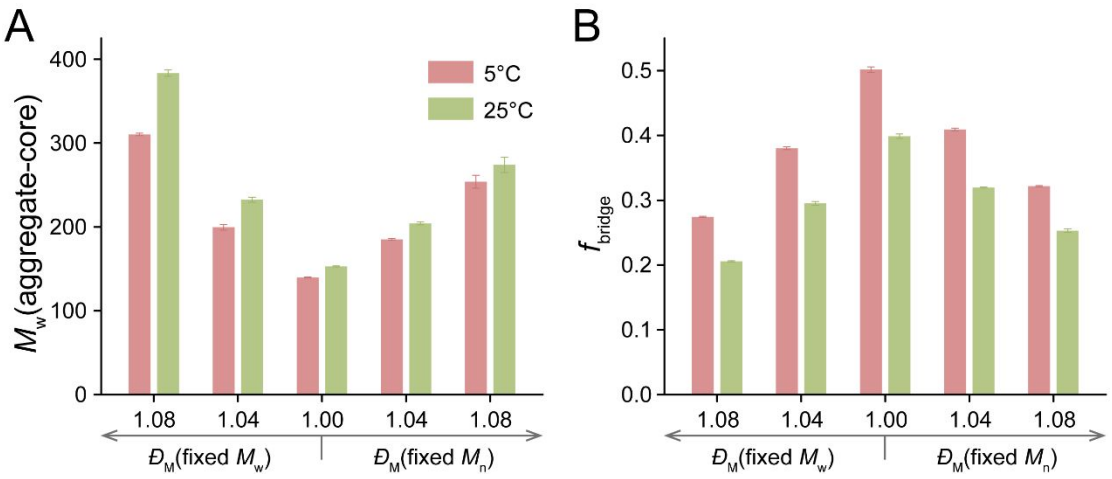

Figure S28. Micelle size and bridge fraction of systems with dispersed hydrophilic blocks. Three components here were $A_{20}B_4A_{20}$, $A_{20}B_{24}A_{20}$, and $A_{20}B_{44}A_{20}$. (A) M_w(aggregate-core) of different systems at indicated temperatures; (B) Bridge fractions of different systems at indicated temperatures. For all systems, $\varphi = 0.25$.

S2.18 $Đ_M$-M_w diagram of fixing hydrophilic blocks (B_y = B_{16}) but changing hydrophobic blocks

The data of systems with chain models of $A_8B_{16}A_8$, $A_{24}B_{16}A_{24}$, and $A_{40}B_{16}A_{40}$, as well as some data from the corresponding monodispersed systems, were summarized in a $Đ_M$-M_w diagram. The results are shown in Figure S29.

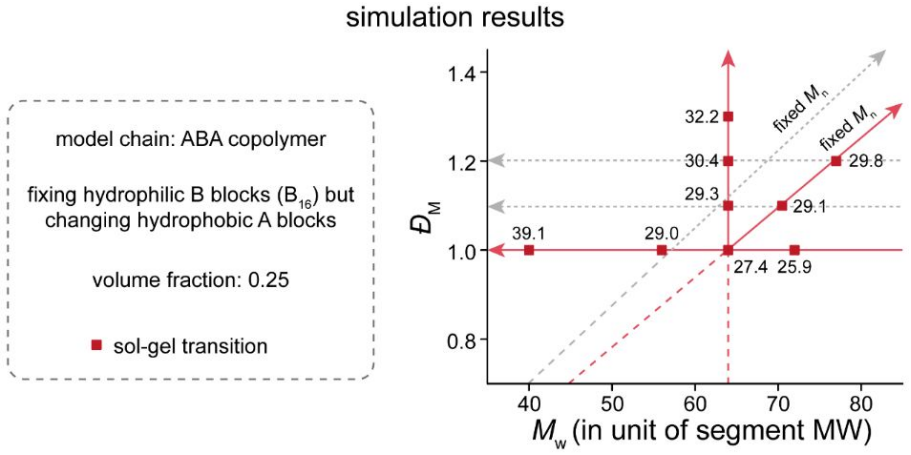

Figure S29. Map of T_{gel} of the indicated systems with $Đ_M$ and M_w as independent coordination axes in simulations. The solid red squares represent systems with sol-gel

transition upon heating, and the numbers near the squares indicate the T_{gel} values of the corresponding systems in units of Celsius degree. The arrow direction means the increase of the T_{gel} or the weakening of the aggregation. The state of the system was determined by the M_w(aggregate-total)-T curve and the S-T curve. Three components here were $A_8B_{16}A_8$, $A_{24}B_{16}A_{24}$, and $A_{40}B_{16}A_{40}$. For all systems, $\varphi = 0.25$.

S2.19 Molecular parameters of copolymers in experiments

Some experimental data from Macromolecules 2014 (ref. 11 in the main manuscript) and some of our unpublished data at that time are employed to compare with the simulation results. The copolymer parameters in experiments are listed in Table S1.

Table S1. Experimental molecular parameters of copolymer PLGA-PEG-PLGA

sample	M_w[a]	M_n[b]	$Đ_M$[c]
C1	5733	1880-1500-1880	1.09
C2	5832	1640-1500-1640	1.22
C3	5766	1520-1500-1520	1.27
C4	5866	1330-1500-1330	1.41
C5	6425	1820-1500-1820	1.25
C6	6450	1570-1500-1570	1.39
C7	5208	1420-1500-1420	1.20
C8	6098	1770-1500-1770	1.21

[a] Calculated from M_n and $Đ_M$; [b] Calculated from proton nuclear magnetic resonance (^{1}H NMR); [c] Measured via gel permeation chromatography (GPC); Data of C1-C5 were from the reference, while data of C6-C8 were unpublished at that time; For all copolymers, the ratio of LA/GA was around 8.

S2.20 Schematic of the $Đ_M$-M_w diagram of fixing hydrophobic blocks but changing hydrophilic blocks

According to the data obtained from Figure 6 in the main manuscript, the schematic $Đ_M$-M_w diagram of fixing hydrophobic blocks but changing hydrophilic blocks are summarized as Figure S30.

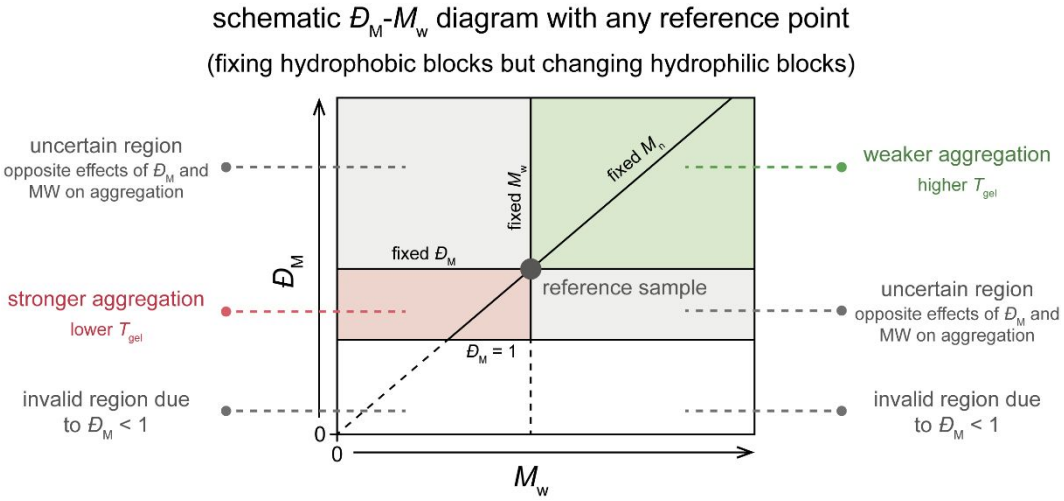

Figure S30. Schematic $Đ_M$-M_w diagram of fixing hydrophobic blocks but changing hydrophilic blocks. The different areas in the $Đ_M$-M_w diagram can tell us the aggregate tendency of other copolymers relative to the reference sample, which can be any sample with any molecular parameter in practice.